To show the location of dendrin in the nucleus in podocytes, triple staining for dendrin, podocalyxin or synaptopodin and DAPI was performed in rat kidney tissues and human kidney tissues. Tissue samples were obtained from diagnostic renal biopsies performed at Juntendo University Hospital. We investigated the samples from patients who had MCD (n=3), membranous nephropathy (MN) (n=3), FSGS (n=4), and lupus nephritis (LN) (n=4) and were manifesting nephrotic-range proteinuria. As control human samples, we used biopsy samples from the patients with minor glomerular abnormalities (n=5). The study was conducted under informed consent and was approved by the ethics committee on human research of the Juntendo University Faculty of Medicine.

Immunoblotting

To check the expression of dendrin, glomeruli were isolated from the kidneys using a graded sieving method [25]. WB analyses for dendrin, and for GAPDH as the internal control, were performed. Isolated glomeruli were lysed and immunoblotting was performed as described previously [25]. To evaluate the expression of cleaved caspase-3, cultured podocytes were treated with ADR (0.25 μg/ ml) for 0, 3 and 6 hours and WB was performed.

TUNEL assay

To detect apoptotic cells *in vivo*, an ApopTag® Plus Peroxidase *In Situ* Apoptosis Detection Kit (Chemicon international Inc., Temecula, CA) was purchased for the TUNEL assay. The TUNEL assay was performed according to the manufacturer's instructions. TUNEL-positive cells in the non-sclerotic parts of the glomeruli were counted.

Cell culture and treatment with ADR

Conditionally immortalized mouse podocytes were cultured as described previously [23]. To evaluate the reaction to ADR *in vitro*, the cells were treated with 0.01 μg/ml to 1.0 μg/ml of ADR in regular medium for 24, 48 and 72 hours. Immunofluorescence microscopy of cultured podocytes was performed as described previously [20]. Immunostaining of cultured podocytes was performed with anti-dendrin and anti-synaptopodin antibodies and DAPI. For the quantitative analysis of the ADR-mediated nuclear import of dendrin, 2000 cells were counted by confocal microscopy for each experiment.

Measurement of apoptosis by counting apoptotic nuclei with hypoploid DNA

The population of cells with hypoploid DNA was measured as described previously [26]. Briefly, the cells were centrifuged at 1,500 rpm for 5 min and the supernatant was decanted. The cells were chilled at 4 °C, then fixed at a concentration of 1-2 x 10^6

cells/ml in 70% ethanol at -20 ℃. Maintaining cells at -20 ℃ for 20 minutes yielded equivalent results. Prior to staining, cells were centrifuged at 1500 rpm for 5 minutes, washed twice with PBS and decanted. The fixed cells were re-suspended by light vortexing in 100 µl of 1 mg/ml RNase (Sigma Chemical Co., St. Louis, MO) solution at 37 ℃ for 20 minutes and were stained with 1 µl of propidium iodide (PI) (500 mg/ ml; Sigma Chemical Co., St. Louis, MO)[20].

Measurement of apoptosis by annexin V and PI staining

Apoptotic cells were identified by staining with annexin V and PI [20]. Briefly, cells (6×10^5) were treated with 0.25 µg/ml of ADR for 48 hours, then washed and suspended in a binding solution containing annexin V-biotin, at dilutions recommended by the manufacturer. After 30 minutes, the cells were washed and streptavisin-allophycocyanin (APC; 5 µg/ ml) was added. Following 20 minutes, PI (1 µg/ ml) was added. At least 10,000 cells were analyzed with FACS per sample. Early apoptosis, late apoptosis and whole apoptosis were determined as the percentages of annexin V+/ PI-, annexin V+/ PI+ and annexin V+ cells.

Statistical analysis

All values were expressed as the mean ± SE. Statistical significance (defined as $P<0.05$) was evaluated using a Tukey-Kramer test, Fisher's PLSD or t-test.

Bioorganic & Medicinal Chemistry Letters 20 (2010) 5839–5842

Contents lists available at ScienceDirect

Bioorganic & Medicinal Chemistry Letters

journal homepage: www.elsevier.com/locate/bmcl

Structure–activity relationship of boronic acid derivatives of tyropeptin: Proteasome inhibitors

Takumi Watanabe [a,*], Hikaru Abe [a], Isao Momose [b], Yoshikazu Takahashi [a], Daishiro Ikeda [b], Yuzuru Akamatsu [a]

[a] Institute of Microbial Chemistry, Tokyo, 3-14-23 Kamiosaki, Shinagawa-ku, Tokyo 141-0021, Japan
[b] Institute of Microbial Chemistry, Numazu, 18-24 Miyamoto, Numazu 410-0301, Japan

ARTICLE INFO

Article history:
Received 20 July 2010
Revised 26 July 2010
Accepted 27 July 2010
Available online 1 August 2010

Keywords:
Proteasome inhibitor
Boronic acid
Structure–activity relationship
Cytotoxicity
Multiple myeloma
Tyropeptin

ABSTRACT

The structure–activity relationship of the boronic acid derivatives of tyropeptin, a proteasome inhibitor, was studied. Based on the structure of a previously reported boronate analog of tyropeptin (**2**), 41 derivatives, which have varying substructure at the N-terminal acyl moiety and P2 position, were synthesized. Among them, 3-phenoxyphenylacetamide **6** and 3-fluoro picolinamide **22** displayed the most potent inhibitory activity toward chymotryptic activity of proteasome and cytotoxicity, respectively. The replacement of the isopropyl group in the P2 side chain to H or Me had negligible effects on the biological activities examined in this study.

Proteasome, a multicatalytic threonine protease, is responsible for ubiquitin-dependent nonlysosomal proteolysis.[1] This enzyme has three distinct active sites that are individually responsible for the chymotrypsin-like, caspase-like, and trypsin-like proteolytic activities.[2] Among these, the chymotrypsin-like activity is of greatest interest, and much research in medicinal chemistry has been focused on it.[3,4]

Elevated levels of the proteasome have been implicated in many diseases including cancer. In fact, it has been reported that the anti-cancer activity of proteasome inhibitors is due to inhibition of the transcriptional factor NF-κB;[5,6] stabilization of p21, p27, and p53;[7,8] and suppression of the unfolded protein response (UPR).[9] Indeed, proteasome inhibitors have been recognized as promising candidates for anti-cancer agent,[10,11] since the US Food and Drug Administration approved the first clinical use of a compound from this class, bortezomib **3** (also referred to as PS-341, Velcade®), for the treatment of multiple myeloma.

Previously, we reported the isolation and structural determination of the novel proteasome inhibitors tyropeptins A (**1**) produced by *Kitasatospora sp.* MK993-dF2,[12,13] and structure–activity relationship (SAR) studies of tyropeptin derivatives.[14,15] In these studies, tyropeptin-boronic acid derivatives (**2** as a representative) were found to exhibit enhanced inhibitory activity against chymotrypsin-like activity of human proteasome when compared to tyropeptin A (Fig. 1).

Encouraged by these results, we conducted further SAR studies of tyropeptin-boronic acid derivatives. In the present study, the effect of acyl moiety located at the N-terminus on the proteasome-inhibitory activity and cytotoxicity against RPMI8226 cells derived from multiple myeloma was investigated. Proteasome-inhibitory activities were determined using purified human erythrocyte-derived 20S proteasome (Enzo Life Sciences. Plymouth Meeting, PA) as previously described.[13]

Scheme 1 summarizes the procedure for synthesizing the tyropeptin-boronic acid derivatives used in this study. According to the method reported previously,[15] 41 analogs of **2** that have a variety of acyl groups at the N-terminus were prepared using WSC·HCl as a coupling reagent with corresponding carboxylic acids and the peptide boronate **4**.[16]

Table 1 shows the inhibitory activity toward proteasome and the cytotoxicity of tyropeptin-boronic acid derivatives synthesized for this study. The almost identical biological activities were observed for the previously reported 1-naphtylacetyl derivative **2** and its regioisomer **5**. The most potent inhibitor of chymotrypsin-like activity was analog **6**, which has a 3-phenoxyphenylacetyl group at the N-terminal acyl moiety; almost ninefold more potent than bortezomib **3** (IC_{50}: 0.0041 for **6** and 0.039 μM for **3**). Unfortunately these compounds showed weak antitumor activity,[17] which prompted us to use different acyl groups. Instead, we chose

* Corresponding author. Tel.: +81 3 3441 4173; fax: +81 3 3441 7589.
E-mail address: twatanabe@bikaken.or.jp (T. Watanabe).

0960-894X/$ - see front matter © 2010 Elsevier Ltd. All rights reserved.
doi:10.1016/j.bmcl.2010.07.122

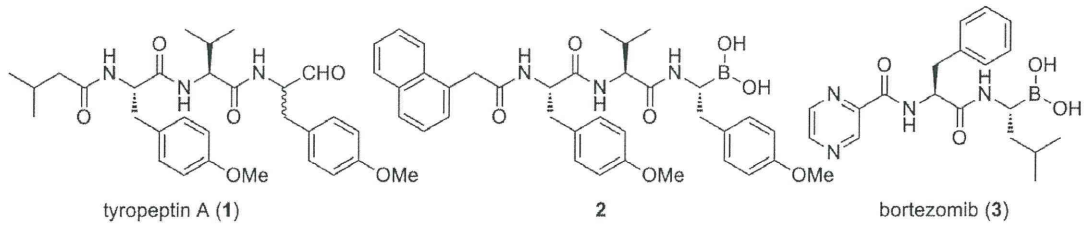

Figure 1. Structure of tyropeptin A (**1**), a tyropeptin-boronic acid derivative (**2**), and bortezomib (**3**).

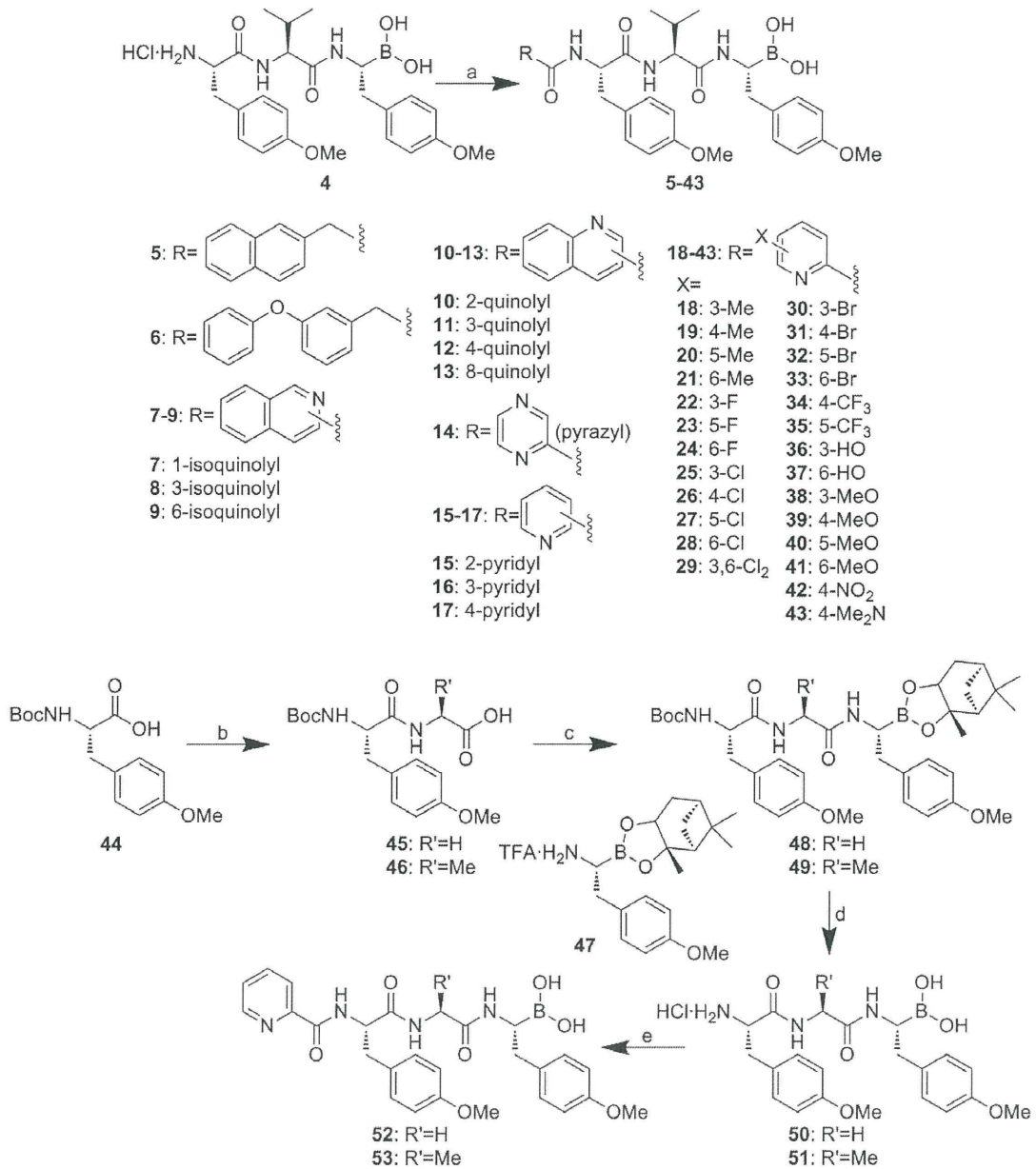

Scheme 1. Reagents and conditions: (a) carboxylic acid, WSC·HCl, HOBt, iPr$_2$NEt, CH_2Cl_2; (b) (i) H-Gly-OBn or H-Ala-OBn, WSC·HCl, HOBt, iPr$_2$NEt, CH_2Cl_2; (ii) H_2, Pd/C, MeOH; (c) **47**, WSC·HCl, HOBt, iPr$_2$NEt, CH_2Cl_2; (d) (i) TFA, $CHCl_3$; (ii) iBuB(OH)$_2$, 1 M HCl, hexane; (e) 2-picolinic acid, WSC·HCl, HOBt, iPr$_2$NEt, CH_2Cl_2.

various N-heteroaromatic rings because bortezomib **3** has a pyrazine carboxamide moiety.

First, amide derivatives of commercially available carboxylic acids having quinoline, isoquinoline, pyrazine, and pyridine nuclei

Table 1
Biological activities of tyropeptin-boronic acid derivatives, and bortezomib (IC_{50}: μM)

Compounds	Chymotrypsin-like activity	Caspase-like activity	Trypsin-like activity	Cytotoxicity (RPMI8226)
5	0.022	39	12	0.17
6	0.0041	29	1.1	0.19
7	0.041	19	10	0.034
8	0.059	11	9	0.093
9	0.38	>40	>40	0.26
10	0.10	16	5.4	0.073
11	0.056	32	10	0.054
12	0.049	24	8.6	0.049
13	0.093	16	18	0.056
14	0.24	33	19	0.017
15	0.23	23	40	0.013
16	0.50	>40	>40	0.87
17	2.3	>40	>40	0.87
18	0.085	>40	20	0.014
19	0.14	30	20	0.014
20	0.12	30	14	0.014
21	0.088	30	17	0.014
22	0.14	25	24	0.0049
23	0.081	30	14	0.019
24	0.11	27	20	0.015
25	0.083	20	20	0.0097
26	0.088	21	15	0.039
27	0.083	16	15	0.039
28	0.10	23	10	0.029
29	0.053	26	13	0.014
30	0.061	20	17	0.013
31	0.095	17	14	0.047
32	0.093	24	14	0.046
33	0.092	27	14	0.044
34	0.15	25	20	0.053
35	0.11	28	19	0.047
36	0.39	29	>40	0.052
37	0.24	>40	11	0.34
38	0.13	26	31	0.041
39	0.087	20	16	0.013
40	0.094	21	14	0.013
41	0.059	35	21	0.051
42	0.19	34	19	0.048
43	0.11	21	15	0.044
52	0.26	34	>40	0.024
53	0.11	>40	>40	0.057
2	0.019	39	>40	0.028
3	0.039	0.75	>40	0.0088

without any substituents were prepared (**7–17**). Except for compound **10**, the quinoline and isoquinoline derivatives inhibited the chymotrypsin-like activity of proteasome more effectively than the pyrazine and pyridine congeners. It is noteworthy that inhibition of proteasome did not necessarily correlate with the cytotoxicity. Indeed, the most potent cytotoxicity, comparable to that of bortezomib, was observed for picolinic acid amide **15**, albeit a modest inhibitory activity against proteasome. Because the analog **15** displayed an antitumor activity in a preliminary experiment,[17] further SAR studies were performed starting with this analog to clarify the effects of substituents on the pyridine ring. To this end, various picolinic groups installed with one (or two in the case of 3,6-dichloroderivative **29**) functional group were introduced at the N-terminus (**18–43**): Me, F, Cl, Br, CF_3, OH, OMe, NO_2, or NMe_2 derivatives.

In most cases, when tested against the chymotrypsin-like activity of proteasome, analogs with additional substituents showed IC_{50} values lower than that of **15** (0.23 μM) except for hydroxylated derivatives **36** and **37** (IC_{50}: 0.39 and 0.24 μM, respectively). In particular, the 3,6-Cl_2 (**29**), 3-Br (**30**), and 6-Me (**41**) derivatives showed comparable potency (IC_{50}: 0.053, 0.061, and 0.059 μM, respectively) to that of bortezomib **3**.

Substantial loss of cytotoxicity toward RPMI8226 was not observed for the compounds of this class. Notably, 3-F derivative **22** displayed one of the most potent cytotoxicities against RPMI8226 among the tyropeptin-related compounds synthesized in our laboratory (IC_{50}: 0.0049 μM). Here again, the potency of the inhibitory activity toward proteasome and cytotoxicity did not coincide with each other. In fact, **22** showed only a moderate activity toward proteasome (IC_{50}: 0.14 μM).

Other than the deleterious effect of an OH group on the inhibition of chymotryptic activity, no obvious relationship was observed between the biological activities examined in this study and the structure of the pyridyl moiety.

In addition, a preliminary study to evaluate the effect of the P2 side chain was conducted. Based on the structure of **15**, two analogs, in which the P2 valine was replaced with either glycine (**52**) or alanine (**53**), were prepared using a procedure that was analogous to the synthesis of the above-mentioned tyropeptin derivatives. As a result, removal of all or part of the P2 side chain of **15** did not influence the biological activity tested in this study.[16]

In summary, boronic acid derivatives of tyropeptin were synthesized and tested for proteasome-inhibitory activity and cytotoxicity against RPMI8226 in this study. The most potent compounds found were 3-phenoxyphenylacetamide **6** (for proteasome-inhibitory activity) and 3-fluoropicolinamide **22** (for cytotoxicity). The structural change in P2 did not affect the in vitro activities tested in this study. In order to clarify whether the structural change of P2 side chain can alter the physicochemical properties of analogs without affecting the biological activities, a SAR study on this moiety is currently under way. Moreover, full details of the antitumor activities of these compounds will be also reported in due course.

Acknowledgments

The authors thank Dr. Ryuich Sawa and Ms. Yumiko Kubota at Institute of Microbial Chemistry, Tokyo, for collecting analytical data. The authors are also grateful to Ms. Shoko Kakuda at Institute of Microbial Chemistry, Numazu, for evaluation of biological activity.

References and notes

1. Ciechanover, A. *Angew. Chem., Int. Ed.* **2005**, *44*, 5944.
2. Kisselev, A. F.; Goldberg, A. L. *Methods Enzymol.* **2005**, *398*, 364.
3. Lopes, U. G.; Erhardt, P.; Yao, R.; Cooper, G. M. *J. Biol. Chem.* **1997**, *272*, 12893.
4. An, B.; Goldfarb, R. H.; Siman, R.; Dou, Q. P. *Cell Death Differ.* **1998**, *5*, 1062.
5. Frankel, A.; Man, S.; Elliot, P.; Adams, J.; Kerbel, R. S. *Clin. Cancer Res.* **2000**, *6*, 33719.
6. Sunwoo, J. B.; Chen, Z.; Dong, G.; Yeh, N.; Bancroft, C. C.; Sausville, E.; Adams, J.; Elliot, P.; Van Waes, C. *Clin. Cancer Res.* **2001**, *7*, 1419.
7. Hideshima, T.; Richardson, P.; Chauhau, D.; Palombella, V. J.; Elliot, P. J.; Adams, J.; Anderson, K. C. *Cancer Res.* **2001**, *61*, 3071.
8. Ling, Y.-H.; Liebes, L.; Jiang, J.-D.; Holland, J. F.; Elliot, P. J.; Adams, J.; Muggia, F. M.; Perez-Solar, R. *Clin. Cancer Res.* **2003**, *9*, 1145.
9. Lee, A.-H.; Iwakoshi, N. N.; Anderson, K. C.; Glimcher, L. H. *Proc. Natl. Acad. Sci. U.S.A.* **2003**, *100*, 9946.
10. Sterz, J.; von Metzler, I.; Hahne, J.-C.; Lamottke, B.; Rademacher, J.; Heider, U. *Expert Opin. Invest. Drugs* **2008**, *17*, 879.
11. Yang, H.; Zonder, J. A.; Dou, P. *Expert Opin. Invest. Drugs* **2009**, *18*, 957.
12. Momose, I.; Sekizawa, R.; Hashizume, H.; Kinoshita, N.; Homma, Y.; Hamada, M.; Iinuma, H.; Takeuchi, T. *J. Antibiot.* **2001**, *54*, 997.
13. Momose, I.; Sekizawa, R.; Hirosawa, S.; Ikeda, D.; Naganawa, H.; Iinuma, H.; Takeuchi, T. *J. Antibiot.* **2001**, *54*, 1004.
14. Momose, I.; Umezawa, Y.; Hirosawa, S.; Iinuma, H.; Ikeda, D. *Bioorg. Med. Chem. Lett.* **2005**, *15*, 1867.
15. Watanabe, T.; Momose, I.; Abe, M.; Abe, H.; Sawa, R.; Umezawa, Y.; Ikeda, D.; Takahashi, Y.; Akamatsu, Y. *Bioorg. Med. Chem. Lett.* **2009**, *19*, 2343.
16. All the new compounds showed satisfactory analytical data. The representatives are listed below: **6**: a white powder: mp 102–105 °C; $[\alpha]_D^{20}$ −36.2 (*c* 0.150, $CHCl_3$); IR (KBr) ν_{max} 3294, 1643, 1512, 1250, 1034 cm^{-1}; ^1H NMR (CD_3OD, 600 MHz); δ 7.32 (2H, m), 7.20 (1H, t, J = 7.9 Hz), 7.12 (2H, d, J = 8.6 Hz), 7.08 (1H, m), 7.06 (2H, d, J = 8.6 Hz), 6.94 (2H, d, J = 7.9 Hz), 6.87–6.80 (5H, m), 6.75 (2H, d, J = 8.6 Hz), 4.62 (1H, m), 4.31 (1H, d, J = 7.6 Hz), 3.73 (3H, s), 3.71 (3H, s), 3.40 (2H, d, J = 14.4 Hz), 3.02 (1H, dd, J = 14.1, 5.1 Hz), 2.82–2.74 (2H, m), 2.51 (1H, dd, J = 14.1, 10.0 Hz), 2.07 (1H, m), 0.95–0.92 (6H, m); ^{13}C NMR (CD_3OD, 150 MHz); δ 177.8, 173.8, 173.5, 160.0, 159.7, 158.8,

158.7, 138.6, 133.8, 131.3, 130.91, 130.88, 130.0, 125.1, 124.4, 120.7, 119.9, 118.2, 115.0, 114.9, 56.5, 55.8, 55.70, 55.65, 43.4, 37.8, 37.3, 31.9, 19.4, 18.8; HRMS (ESI-Orbitrap) m/z calcd for $C_{38}H_{44}BN_3NaO_8^+$ [(M+Na)$^+$] 704.3114, found: 704.3096. Compound **15**: a white powder: mp 123–125 °C; $[\alpha]_D^{20}$ −48.0 (c 0.260, $CHCl_3$); IR (KBr) ν_{max} 3305, 1658, 1512, 1246, 1176, 1034 cm^{-1}; ^{1}H NMR (CD_3OD, 600 MHz); δ 8.60 (1H, m), 8.00 (1H, m), 7.92 (1H, dt, J = 7.7, 1.8 Hz), 7.53 (1H, m), 7.16–7.13 (4H, m), 6.85 (2H, d, J = 8.7 Hz), 6.78 (2H, d, J = 8.7 Hz), 4.36 (1H, d, J = 8.0 Hz), 3.74 (3H, s), 3.71 (3H, s), 3.16 (1H, dd, J = 13.9, 5.2 Hz), 2.98 (1H, dd, J = 13.9, 8.5 Hz), 2.90 (1H, m), 2.84 (1H, dd, J = 14.2, 5.5 Hz), 2.53 (1H, dd, J = 14.2, 10.0 Hz), 2.13 (1H, m), 1.00 (3H, d, J = 6.2 Hz), 0.99 (3H, d, J = 6.2 Hz); ^{13}C NMR (CD_3OD, 150 MHz); δ 177.6, 173.6, 166.1, 160.1, 159.7, 150.4, 149.8, 138.8, 133.8, 131.4, 130.8, 129.7, 128.0, 123.1, 115.0, 114.9, 56.6, 55.9, 55.7, 55.6, 38.4, 37.2, 31.9, 19.4, 18.9; HRMS (ESI-TOF) m/z calcd for $C_{30}H_{37}BN_4NaO_7^+$ [(M+Na)$^+$] 599.2648, found: 599.2639. Compound **22**: a white powder: mp 126–128 °C; $[\alpha]_D^{20}$ −39.8 (c 0.215, $CHCl_3$); IR (KBr) ν_{max} 3305, 1658, 1512, 1246, 1176, 1034 cm^{-1}; ^{1}H NMR (CD_3OD, 600 MHz); δ 8.60 (1H, m), 7.74–7.70 (1H, m), 7.64–7.61 (1H, m), 7.17 (2H, d, J = 8.6 Hz), 7.09 (2H, d, J = 8.6 Hz), 6.83 (2H, d, J = 8.6 Hz), 6.71 (2H, d, J = 8.6 Hz), 4.36 (1H, d, J = 7.2 Hz), 3.74 (3H, s), 3.72 (3H, s), 3.10–3.03 (2H, m), 2.84 (1H, dd, J = 8.9, 6.2 Hz), 2.76 (1H, dd, J = 14.2, 6.2 Hz), 2.54 (1H, dd, J = 14.2, 8.9 Hz), 2.07 (1H, m), 2.13 (1H, m), 0.84 (3H, d, J = 6.5 Hz), 0.81 (3H, d, J = 6.5 Hz); ^{13}C NMR (CD_3OD, 150 MHz); δ 178.0, 173.7, 164.3 (d, J = 5.7 Hz), 160.5 (d, J = 268.6 Hz), 160.3, 159.6, 145.9 (d, J = 5.7 Hz), 138.6 (d, J = 5.7 Hz), 133.9, 131.5, 130.9, 130.1 (d, J = 5.7 Hz), 129.6, 127.5 (d, J = 20.1 Hz), 115.1, 114.9, 56.9, 56.2, 55.71, 55.69, 38.7, 37.0, 31.1, 19.4, 18.6; HRMS (ESI-Orbitrap) m/z calcd for $C_{30}H_{36}BFN_4NaO_7^+$ [(M+Na)$^+$] 617.2553, found: 617.2568.

17. Manuscript in preparation.

Published OnlineFirst July 14, 2010; DOI:10.1158/0008-5472.CAN-10-0184

Cancer Research

Circadian Rhythm of Transferrin Receptor 1 Gene Expression Controlled by c-Myc in Colon Cancer –Bearing Mice

Fumiyasu Okazaki, Naoya Matsunaga, Hiroyuki Okazaki, et al.

Cancer Res 2010;70:6238-6246. Published OnlineFirst July 14, 2010.

Published OnlineFirst July 14, 2010; DOI:10.1158/0008-5472.CAN-10-0184

Molecular and Cellular Pathobiology

Cancer Research

Circadian Rhythm of Transferrin Receptor 1 Gene Expression Controlled by c-Myc in Colon Cancer–Bearing Mice

Fumiyasu Okazaki[1], Naoya Matsunaga[1], Hiroyuki Okazaki[1], Naoki Utoguchi[2], Ryo Suzuki[2], Kazuo Maruyama[2], Satoru Koyanagi[1], and Shigehiro Ohdo[1]

Abstract

The abundance of cell surface levels of transferrin receptor 1 (TfR1), which regulates the uptake of iron-bound transferring, correlates with the rate of cell proliferation. Because TfR1 expression is higher in cancer cells than in normal cells, it offers a target for cancer therapy. In this study, we found that the expression of TfR1 in mouse colon cancer cells was affected by the circadian organization of the molecular clock. The core circadian oscillator is composed of an autoregulatory transcription-translation feedback loop, in which CLOCK and BMAL1 are positive regulators and the *Period* (*Per*), *Cryptochrome* (*Cry*), and *Dec* genes act as negative regulators. TfR1 in colon cancer–bearing mice exhibited a 24-hour rhythm in mRNA and protein levels. Luciferase reporter analysis and chromatin immunoprecipitation experiments suggested that the clock-controlled gene *c-MYC* rhythmically activated the transcription of the *TfR1* gene. Platinum incorporation into tumor DNA and the antitumor efficacy of transferrin-conjugated liposome-delivered oxaliplatin could be enhanced by drug administration at times when TfR1 expression increased. Our findings suggest that the 24-hour rhythm of TfR1 expression may form an important aspect of strategies for TfR1-targeted cancer therapy. *Cancer Res; 70(15); 6238–46. ©2010 AACR.*

Introduction

In mammals, the master pacemaker controlling the circadian rhythm is located in the suprachiasmatic nuclei of the hypothalamus (1). Regulation of circadian physiology relies on the interplay of interconnected transcription-translation feedback loops. The BMAL1/CLOCK complex activates clock-controlled genes, including *Per, Cry*, and *Dec*, the products of which act as repressors by interacting with BMAL1/CLOCK (2–5). This mechanism also regulates the 24-hour rhythm in output physiology through the periodic activation/repression of clock-controlled output genes in healthy peripheral tissue and tumor tissue (6, 7).

Transferrin receptor 1 (TfR1) is involved in the uptake of iron into cells through the binding and internalization of transferrin, and its regulation by intracellular iron levels has assisted in the elucidation of many important aspects of cellular iron homeostasis (8, 9). Iron is important for metabolism, respiration, and DNA synthesis. Thus, TfR1 is expressed not only in normal healthy cells but also in malignant tumor cells (8, 10). Recently, another TfR-like molecule named TfR2 has been recognized and investigated (11, 12), but the exact function of TfR2 remains unclear (8). It has been reported that the expression of TfR1 in mammary epithelial cells exhibits a significant 24-hour rhythm (13). Such rhythmic variation in TfR1 expression seems to affect its iron uptake function resulting in time-dependent changes in the internalization of iron-loaded Tf. However, it is not clear if the expression of TfR1 in colon cancer cells shows a significant 24-hour rhythm.

Many of the pharmacologic properties of conventional drugs can be improved through the use of an optimized drug delivery system (DDS), which includes particular carriers composed primarily of lipids and/or polymers (14). The high expression of TfR1 in tumor can potentially be used to deliver cytotoxic agents into malignant cells, including chemotherapeutic drugs, cytotoxic proteins (8), and Tf-coupled polyethylene glycol (Tf-PEG) liposomes were designed as intracellular targeting carriers for drugs by systemic administration. In fact, Tf-PEG liposomes encapsulating a platinum (Pt)-based anticancer drug, oxaliplatin, can increase its accumulation in tumor masses (15, 16). On the other hand, daily rhythmic variations in biological functions are thought to affect the efficacy and/or toxicity of drugs: a large number of drugs cannot be expected to have the same potency at different administration times (7, 17). However, it is unclear what influence the rhythmic expression of TfR1 has on the pharmacokinetics/pharmacodynamics of transferrin targeting liposomes.

Authors' Affiliations: [1]Department of Pharmaceutics, Graduate School of Pharmaceutical Sciences, Kyushu University, Fukuoka, Japan and [2]Department of Pharmaceutics, Teikyo University, Sagamiko, Sagamihara, Japan

Note: Supplementary data for this article are available at Cancer Research Online (http://cancerres.aacrjournals.org/).

F. Okazaki, N. Matsunaga, and S. Ohdo contributed equally to this work.

Corresponding Author: Shigehiro Ohdo, Department of Pharmaceutics, Graduate School of Pharmaceutical Sciences, Kyushu University, Fukuoka, 812-8582, Japan. Phone: 81-92-642-6610; Fax: 81-92-642-6614; E-mail: ohdo@phar.kyushu-u.ac.jp.

doi: 10.1158/0008-5472.CAN-10-0184

Published OnlineFirst July 14, 2010; DOI:10.1158/0008-5472.CAN-10-0184

In this study, we found that the circadian expression of *c-Myc*, which is controlled by the circadian clock, affects *TfR1* gene transcription in colon cancer cells. The levels of *TfR1* mRNA and protein exhibited a 24-hour oscillation in tumor cells implanted in mice. Thus, to evaluate the rhythmic function of TfR1 and the utility for TfR1-targeting cancer therapy, we investigated how the rhythmic variation in TfR1 production influenced the pharmacologic efficacy of TfR1-targeting liposomal DDS.

Materials and Methods

Animals and cells

Seven-week-old male BALB/c mice (Charles River Japan) were housed with lights on from 7:00 a.m. to 7:00 p.m. at a room temperature of 24 ± 1°C and a humidity of 60 ± 10% with food and water *ad libitum*. Colon 26 cells (Cell Resource Center for Biomedical Research, Tohoku University) were maintained in RPMI 1640 supplemented 10% fetal bovine serum (FBS) at 37°C in a humidified 5% CO_2 atmosphere. A 25-μL volume with 2×10^7 viable tumor cells was inoculated into the right hind footpad of each mouse. The tumor volume was estimated according to a formula that has been described previously (7). Tissue slices of the removed tumor masses were made, and the tumor tissue was confirmed histopathologically.

Experimental design

To assess the temporal expression profile of TfR1 in tumor cells, tumor masses were removed from individual tumor-bearing mice at six different time points (9:00 a.m., 1:00 p.m., 5:00 p.m., 9:00 p.m., 1:00 a.m., and 5:00 a.m.) 7 days after the implantation of tumor cells. The levels of *TfR1* protein and mRNA were measured by Western blotting analysis and quantitative reverse transcription-PCR (RT-PCR), respectively. To investigate how the rhythmic variation in *TfR1* expression occurs in tumor cells, the influence of CLOCK/BMAL1 and c-MYC on the transcriptional activity of the *TfR1* gene was assessed using luciferase reporter constructs containing wild-type E-box or mutated E-box of the mouse *TfR1* promoter, which was based on previous reports. To elucidate the role of c-MYC in the control of the rhythmic expression of *TfR1*, endogenous c-MYC in Colon 26 cells was downregulated by small interfering RNA (siRNA). The c-MYC–downregulated cells were treated with 50% FBS for 2 hours to synchronize their circadian clock, and the mRNA levels of *TfR1* were assessed at 44, 48, 52, 56, 60, 64, and 68 hours after 50% serum treatment. In the same manner as described above, the protein levels of c-MYC and CLOCK were assessed by Western blotting analysis. To explore the temporal binding of endogenous c-MYC and CLOCK to the E-box in the mouse *TfR1* gene, chromatin immunoprecipitation analysis was performed in individual tumor masses at 9:00 a.m. and 9:00 p.m. To investigate the function of the 24-hour oscillation of TfR1 expression, time-dependent changes in Pt internalization into tumor cells were assessed using Tf-coupled liposomes encapsulating oxaliplatin (Tf-NGPE L-OHP). The cultured Colon 26 cells were treated with 50% FBS as described above and then harvested for RNA extraction at 0, 6, 12, 18, and 24 hours after 50% FBS treatment. Nontreated Colon 26 cells harvested at the same time points were used as the control. At 6 or 18 hours after serum treatment, cells were exposed to Tf-NGPE L-OHP (L-OHP, 0.4 mg/mL) for 3 hours. The Pt content in the DNA was measured using an inductively coupled plasma mass spectrometer (ICP-MS). To explore the dosing time–dependent difference in the internalization of Pt into tumor cells *in vivo*, tumor-bearing mice were injected with a single dose of Tf-NGPE L-OHP at 9:00 a.m. or 9:00 p.m. Plasma and tumor DNA samples were collected only once from individual mice at 1, 3, and 6 hours after injection. The plasma concentration of Pt and its content in tumor DNA were measured as described above. Then, tumor volumes were measured throughout the duration of the experiment.

RT-PCR analysis

Total RNA was extracted using RNAiso (TaKaRa). The cDNAs of mouse *TfR1* (NM011638), *TfR2* (NM015799), *c-Myc* (NM010849), and β-*actin* (NM007393) were synthesized using PrimeScript Reverse Transcriptase (TaKaRa), and the synthesized cDNAs were amplified using GoTaq Green Master Mix (Promega). The PCR products were run on 2% agarose gels. After staining with ethidium bromide, the gel was photographed using Polaroid-type film. The density of each band was analyzed using NIH image software on a Macintosh computer. To evaluate the quantitative reliability of RT-PCR, kinetic analysis of the amplified products was performed to ensure that signals were derived only from the exponential phase of amplification, as previously described (7, 17). We evaluated the validity of our semiquantitative PCR methods using real-time PCR. cDNA was prepared by reverse transcription of total RNA. Real-time PCR analysis was performed on diluted cDNA samples with SYBR Premix Ex Taq Perfect Real-Time (TaKaRa) using a 7500 Real-time PCR system (Applied Biosystems). In addition, as confirmation of RNA extraction from each tumor cell sample, the expression level of *Vegf* mRNA was measured (Supplementary Data S1).

Western blotting analysis

Nuclear or cytoplasmic proteins in tumor masses were extracted using NE-PER Nuclear and Cytoplasmic Extraction Reagents (Pierce Biotechnology). The protein concentrations were determined using a BCA Protein Assay kit (Pierce Biotechnology). The lysate samples were separated on 6% or 10% SDS-polyacrylamide gels and transferred to polyvinylidene difluoride membranes. The membranes were reacted with antibodies against TfR1 (Zymed Laboratories), c-MYC, CLOCK, β-actin (Santa Cruz Biotechnology), or RNA pol II (Abcam). The immunocomplexes were further reacted with horseradish peroxidase–conjugated secondary antibodies and visualized using Super Signal Chemiluminescent Substrate (Pierce Biotechnology). The membranes were photographed using Polaroid-type film, and the density of each band was analyzed using NIH image software on a Macintosh computer.